Applied Surface Science 255 (2009) 9566–9571

Contents lists available at ScienceDirect

Applied Surface Science

journal homepage: www.elsevier.com/locate/apsusc

Early stage expansion and time-resolved spectral emission of laser-induced plasma from polymer

Myriam Boueri [a], Matthieu Baudelet [a,1], Jin Yu [a,*], Xianglei Mao [b], Samuel S. Mao [b], Richard Russo [b]

[a] Université de Lyon, F-69622 Lyon, Université Lyon 1, Villeurbanne, CNRS, UMR5579, LASIM, France
[b] Lawrence Berkeley National Laboratory, Berkeley, CA, USA

ARTICLE INFO

Article history:
Available online 21 April 2009

PACS:
52.38.Mf (laser ablation)
52.38.Dx (laser light absorption in plasmas (collisional, parametric, etc.))
52.35.Tc (shock waves and discontinuities)

Keywords:
Laser ablation of polymer
Early stage plasma expansion
Plasma spectral emission

ABSTRACT

In the nanosecond laser ablation regime, absorption of laser energy by the plasma during its early stage expansion critically influences the properties of the plasma and thus its interaction with ambient air. These influences can significantly alter spectral emission of the plasma. For organic samples especially, recombination of the plasma with the ambient air leads to interfering emissions with respect to emissions due to native species evaporated from the sample. Distinguishing interfering emissions due to ambient air represents a critical issue for the application of laser-induced breakdown spectroscopy (LIBS) to the analysis of organic materials. In this paper, we report observations of early stage expansion and interaction with ambient air of the plasma induced on a typical organic sample (nylon) using time-resolved shadowgraph. We compare, in the nanosecond ablation regime, plasmas induced by infrared (IR) laser pulses (1064 nm) and ultraviolet (UV) laser pulses (266 nm). Nanosecond ablation is compared with femtosecond ablation where the post-ablation interaction is absent. Subsequent to the early stage expansion, we observe for each studied ablation regime, spectral emission from CN, a typical radical for organic and biological samples. Time-resolved LIBS allows identifying emissions from native molecular species and those due to recombination with ambient air through their different time evolution behaviors.

1. Introduction

Laser-induced breakdown spectroscopy (LIBS) has been demonstrated as a powerful analytical technique for various types of samples, gas, aerosols, soils, minerals, or alloys [1,2]. The extension of this technique to the analysis of organic or biological materials still remains a challenging task, although several groups demonstrated the potentials of LIBS for detection and identification of explosives or biological hazards [3–8]. A crucial step for such extension is certainly a detailed understanding of the laser ablation plasma induced from organic or biological materials. The mechanisms of mass transfer from sample to plasma as well as the interaction between plasma and ambient air need to be extensively studied in order to extract, from emission spectra, suitable analytical data for characterizing the analyzed sample. Compared to the analysis of metallic samples, the analysis of organic samples with LIBS under atmospheric pressure is much more sensitive to interaction between the plasma and the ambient air, since such interaction leads to interfering emissions from organic elements and compounds such as O, N, or CN resulting from the dissociation of air molecules or the recombination between plasma and air [9,10].

In this paper, we present a time-resolved study of a laser ablation plasma induced from a polymer (nylon) sample in atmospheric air. Through a detailed study of the plasma in different ablation regimes, the purpose of this study is to identify a suitable regime for an optimized LIBS analysis of organic or biological materials. The time scale of plasma evolution was divided into two parts: from the impact of the laser pulse on the sample surface to several tens of nanoseconds, the early stage of plasma expansion was observed by time-resolved pump-probe shadowgraph. Time-resolved LIBS was then used to observe the evolution of spectral emission, especially the emission from diatomic molecular radicals such as CN, from the plasma up to several μs. Continuous observation over these two time intervals allows us to correlate the early stage expansion and the interaction with ambient air of the plasma to its spectral emission detected in LIBS. Different regimes of ablation in terms of laser pulse duration (nanosecond or femtosecond), wavelength (IR or UV) and fluence

* Corresponding author at: Laboratoire de Spectrométrie Ionique et Moléculaire, UMR CNRS 5579, Université Claude Bernard Lyon 1, 43, Bd. du 11 Novembre 1918, F-69622 Villeurbanne Cedex, France. Tel.: +33 4 72 44 81 78; fax: +33 4 72 34 15 07.
E-mail address: jin.yu@lasim.univ-lyon1.fr (J. Yu).
[1] Actual address: CREOL, The College of Optics & Photonics, University of Central Florida, P.O. Box 162700, Orlando, FL 32816-2700, USA.

0169-4332/$ – see front matter © 2009 Elsevier B.V. All rights reserved.
doi:10.1016/j.apsusc.2009.04.088

are systematically studied and compared in order to identify suitable ablation regimes to improve the analytical abilities of LIBS for organic or biological materials using molecular emission spectroscopy.

2. Experimental setup

In our experiments, Nylon 6,6 was used as a typical organic sample because it contains native CN molecular radicals. In our previous work, we have demonstrated that native CN radicals can be used as a marker for biological materials thanks to its strong emission around 388 nm. However, in a LIBS spectrum of an organic material, emission from native CN radicals ablated from the sample has to be distinguished with that from CN radicals due to recombination between plasma and ambient air [9,11]. Nylon presents also good mechanical properties for sample preparation with a good quality flat surface.

Early stage plasma expansion was observed using a typical time-resolved pump-probe shadowgraph setup. In the nanosecond regime, the ablation beam was provided by a 10 Hz Nd:YAG laser which emitted in the fundamental (1064 nm) or in the fourth harmonic (266 nm). Pulse energy ranged from 1 mJ to 5 mJ with pulse duration of 4 ns. A quartz lens of focal length 50 mm focused the laser pulses on the surface of the sample. The position of the laser beam waist was carefully adjusted in order to obtain a beam size of 100 μm in diameter on the sample surface. Ablation craters were measured using a white light interferometer (Zygo, NewView 200) to confirm that the beam was the same diameter when laser parameters (wavelength, energy) were changed. The resulted fluences ranged from 12.7 J/cm^2 to 63.7 J/cm^2. For the femtosecond ablation regime, a 10 Hz chirped pulse amplified (CPA) Ti:Sapphire laser (800 nm) was used in the same fluence range with a pulse duration of 100 fs.

The probe beam crossed the ablation beam at a right angle. It consisted of one part of the beam provided by the CPA Ti:Sapphire laser. Pulses of about 10 μJ energy were doubled to 400 nm by passing through a KDP crystal. Natural divergence of the beam allowed it to cross the plasma plume with an enlarged section in such way that the plasma was illuminated with a uniform blue beam. Detection of the shadow induced by the plasma was performed using a CCD camera equipped with a narrow band blue filter.

The synchronization between ablation and probe pulses was realized in the nanosecond ablation regime with electronic delay between the Q-switches of the nanosecond laser and the regenerative amplifier of the femtosecond laser. Due to the uncertainty of pulse ejection time with respect to the Q-switch of the regenerative amplifier, actual delay between the nanosecond ablation pulse and the femtosecond probe pulse was measured with two fast photodiodes detecting scattered light from nano and femtosecond pulses. A fast oscilloscope measured the time delay between the two electric pulses corresponding to the two laser pulses for each ablation event. In the femtosecond ablation regime, delay for the probe pulse was generated with an optical delay line. Our pump-probe shadowgraph was able to observe the expansion of the plasma from its initiation to a delay of several tens of ns with a time resolution of several nanoseconds for the nanosecond ablation regime (limited by the response time of the photodiodes used). The time resolution for the femtosecond ablation configuration was in the picosecond range.

From about 100 ns after the laser impact on the sample surface up to a delay of several μs, optical emission from the plasma was detected with time-resolved LIBS. The setup used was a typical LIBS setup with a detection system including an Echelle spectrometer coupled to an ICCD camera. Electronic gating on the ICCD allowed a time resolution of 10 ns. In our experiments, nylon samples cut from a same piece of Nylon 6,6 were ablated with laser pulses with different parameters (pulse duration, wavelength, and energy). Shadowgraph pictures corresponded to single shot images, while time-resolved LIBS signals were accumulated over 200 laser shots to increase the signal to noise ratio. The sample was moved during the measurements in order to ensure a fresh surface for each laser shot.

3. Experimental results and discussions

3.1. Early stage expansion of plasma in the nanosecond ablation regime

Fig. 1 shows shadowgraphs of plasmas induced on the surface of a nylon sample by nanosecond IR (1064 nm) laser pulses, with pulse energies of 1, 3 and 5 mJ (Fig. 1a, b and c, respectively) corresponding to fluences of 12.7 J/cm^2, 38.1 J/cm^2 and 63.7 J/cm^2. The corresponding shadowgraphs for nanosecond UV (266 nm) ablation are shown in Fig. 2.

Comparing shockwave expansion of these two ablation regimes, we remark that in the UV regime, shockwaves globally expand in spherical wave for weak as well for high fluences. Shockwave expansion in the IR regime is clearly anisotropic. Expansion backward along the laser pulse propagation direction is faster than transversal expansion. The anisotropy becomes more pronounced when the laser pulse energy increases. This anisotropic behavior in the IR regime is due to the laser-supported detonation wave (LSD) [12]. The expanding plasma absorbs energy from the tailing part of the laser pulse, leading to a preferential expansion of the shockwave toward the incoming laser pulse direction. For a given electronic density, this absorption is more efficient for an infrared pulse due to the dependence of the plasma frequency on electron density. In the UV ablation regime, no significant absorption of the laser pulse by the plasma is observed. The shockwave globally expands in an isotropic way. Fig. 4a and b show the height of the shockwave as a function of the delay after laser pulse impact on the sample for nanosecond IR and UV ablation regimes. The heights are measured from shadowgraphs. We can see higher axial expansion velocity for short delays in IR regime due to the LSD, which confirms the above discussion about the anisotropic expansion of the shockwave in the IR ablation regime.

We remark also in Fig. 2 small structures observed for laser pulse energy larger than 3 mJ on the top of spherically expanding shockwaves in the form of a small tip of higher propagation velocity. The appearance of these picks is not regular pulse to pulse. However the tendency is a more frequent appearance for higher laser energies. This structure is quite different from the LSD observed in Fig. 1 for nanosecond IR ablation. Only a small zone on the top of shockwave is affected. And this structure can appear long time after the end of the laser pulse. Because of the high transparency of the plasma for UV radiation, these local picks cannot be due to absorption of laser energy by the plasma. They can however be due to ionized channels induced in air by UV laser pulses before hitting the sample surface. In fact, the probability of photoionization of air molecules (O_2 and N_2) by 266 nm radiation (4.66 eV) becomes important for high laser fluences. The ionization potentials are respectively 12.08 eV and 15.58 eV for O_2 and N_2 [13], which correspond for 266 nm radiation to respectively 3 and 4 photon-transitions. In our experiments, ionized channels become strong enough to be clearly observed by shadowgraph in the UV ablation regime for laser pulse energy larger than 5 mJ. Free electrons from photoionization absorb energy from laser pulse, which leads to heating and transversal expansion of the ionized channel. Propagation of the shockwave is thus accelerated in contact with the ionized channel with lower pressure, which results in a small pick observed on the top of the shockwave. The small size of the high velocity picks is due to the nonlinear power

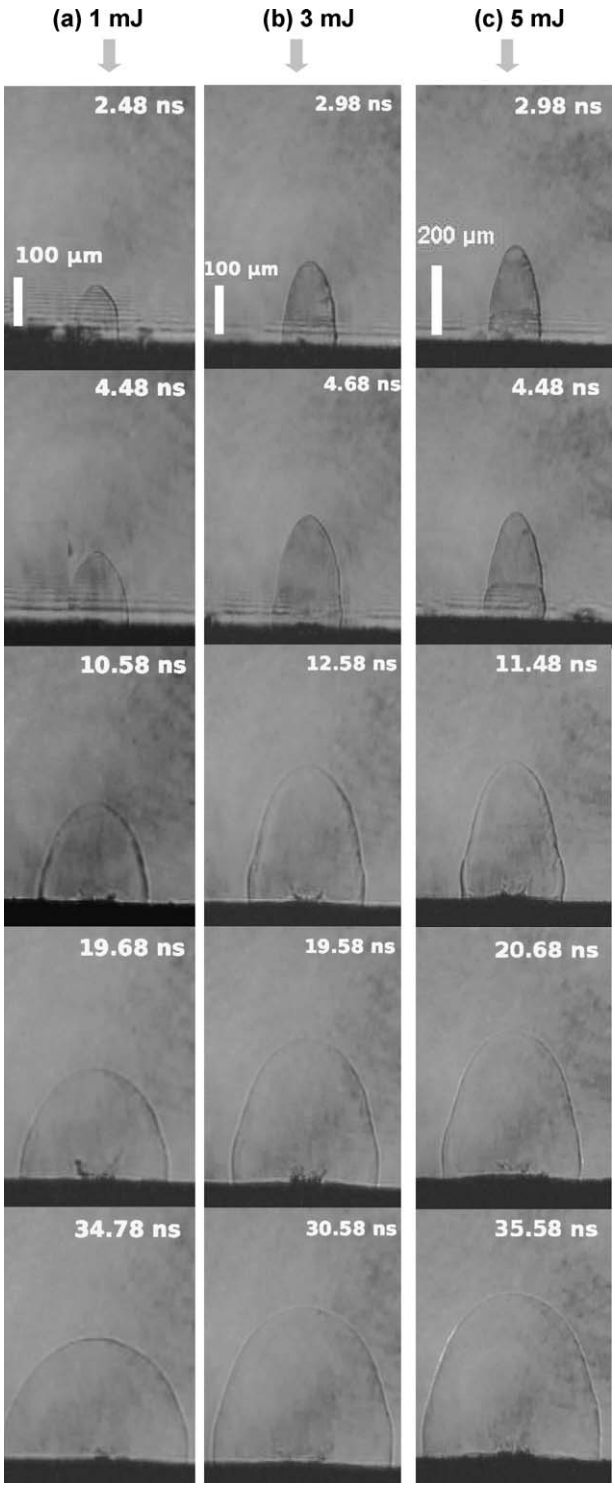

Fig. 1. Shadowgraphs of the plasmas induced on the surface of a nylon sample by nanosecond IR (1064 nm) laser pulses, with pulse energies of 1, 3 and 5 mJ (a, b and c, respectively).

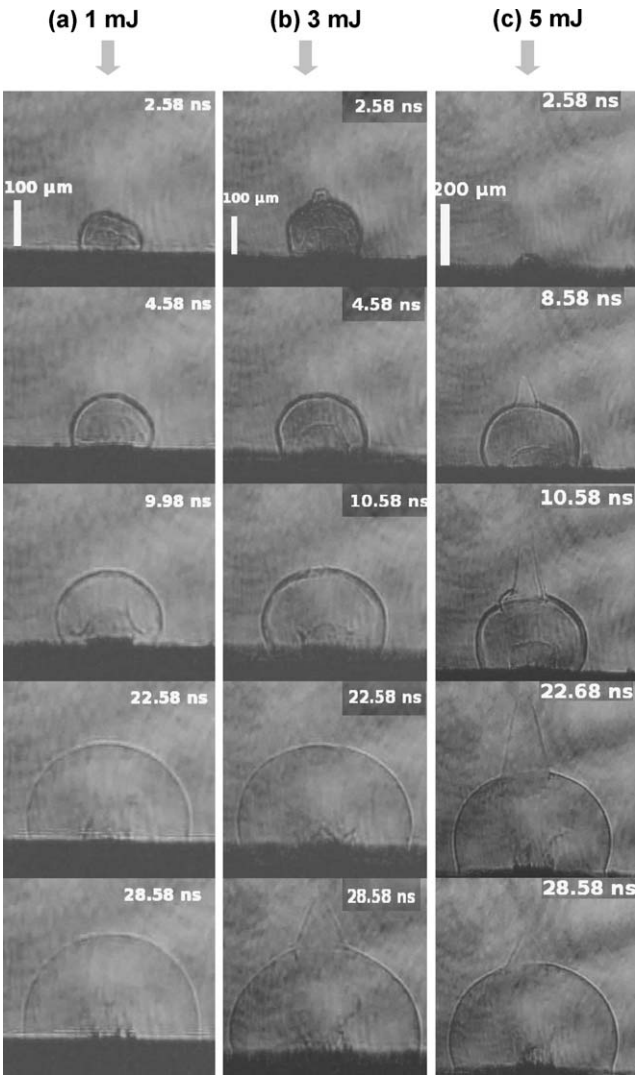

Fig. 2. Shadowgraphs of the plasmas induced on the surface of a nylon sample by nanosecond UV (266 nm) laser pulses, with pulse energies of 1, 3 and 5 mJ (a, b and c, respectively).

dependence of multiphoton absorption probability, which allows high transition rate only in the central part of laser beam section where laser intensity is higher.

3.2. Early stage expansion of plasma in the femtosecond ablation regime

Fig. 3 shows shadowgraphs of plasmas induced on the surface of a nylon sample by femtosecond IR (800 nm) laser pulses, with pulse energies of 1, 3 and 4 mJ (Fig. 3a, b and c, respectively). We remark that the observed shockwave expansions are essentially spherical. That corresponds well to the fact that in the femtosecond ablation regime there is not post-ablation interaction between the plasma and the laser pulse. However high intensity of a femtosecond laser pulse can induce an ionized channel in air before the pulse hits the sample. Such channel can be clearly observed in Fig. 3b and c for pulse energy of 3 and 4 mJ. Due to the ionized channel in air, a tip is observed on the top of a shockwave similar to that observed in the nanosecond UV ablation regime. Compared to shadowgraphs in nanosecond ablation regimes, we can also remark that the shadowgraphs in the femtosecond ablation regime present a higher contrast, which corresponds to a plume with higher density. Fig. 4c shows height of shockwave as a function of the delay after impact of the laser pulse on the sample. Compared to the cases of nanosecond ablation (Fig. 4a and b), one finds a smaller expansion velocity in the femtosecond regime. We can explain this observation by the energy conservation and by the fact that in femtosecond ablation regime, the efficiency of nanoparticle generation is higher. Plasma is generated with a lower degree of atomization in femtosecond ablation [14].

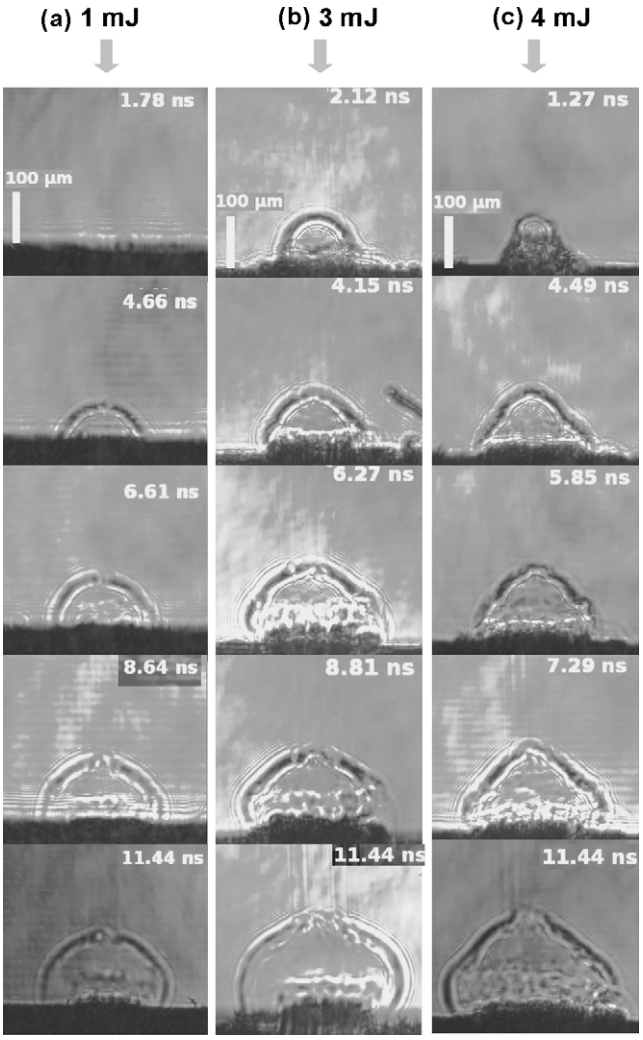

Fig. 3. Shadowgraphs of the plasmas induced on the surface of a nylon sample by femtosecond IR (800 nm) laser pulses, with pulse energies of 1, 3 and 4 mJ (a, b and c, respectively).

3.3. Time-resolved molecular emission from the plasma

The subsequent evolution of the plasma from a delay of about 100 ns to several µs is monitored by time-resolved LIBS. Fig. 5 shows the results of time-resolved observation of the emission from diatomic molecules CN in plasma. Intensity of the band head at 388.3 nm is measured as a function of the delay after the laser pulse impact on the sample for three different regimes of ablation: nanosecond IR (Fig. 5a), nanosecond UV (Fig. 5b), and femtosecond (Fig. 5c), and for three laser pulse energies (1, 3 and 5 mJ). The intensity of the atomic carbon line at 247.9 nm is also plotted in the figure for comparison. Plasma emission was detected for the different ablation regimes in the same condition.

For the intensity of the carbon line, only one type of behavior is observed: the line intensity monotonically decreases although the decay time constant increases as laser pulse energy increases. However the line intensity of CN molecule exhibits two different types of behavior. In different ablation regimes, molecular line intensity can monotonically decrease, or undergo an initial increasing phase before a subsequent decay. We have demonstrated in our previous works that monotonic intensity decay indicates the emission from native CN molecules directly ablated from the sample. Such native CN molecules can be used as a marker of biological materials or organic materials containing CN bonds like nylon [9]. The initial increase of emission intensity from CN

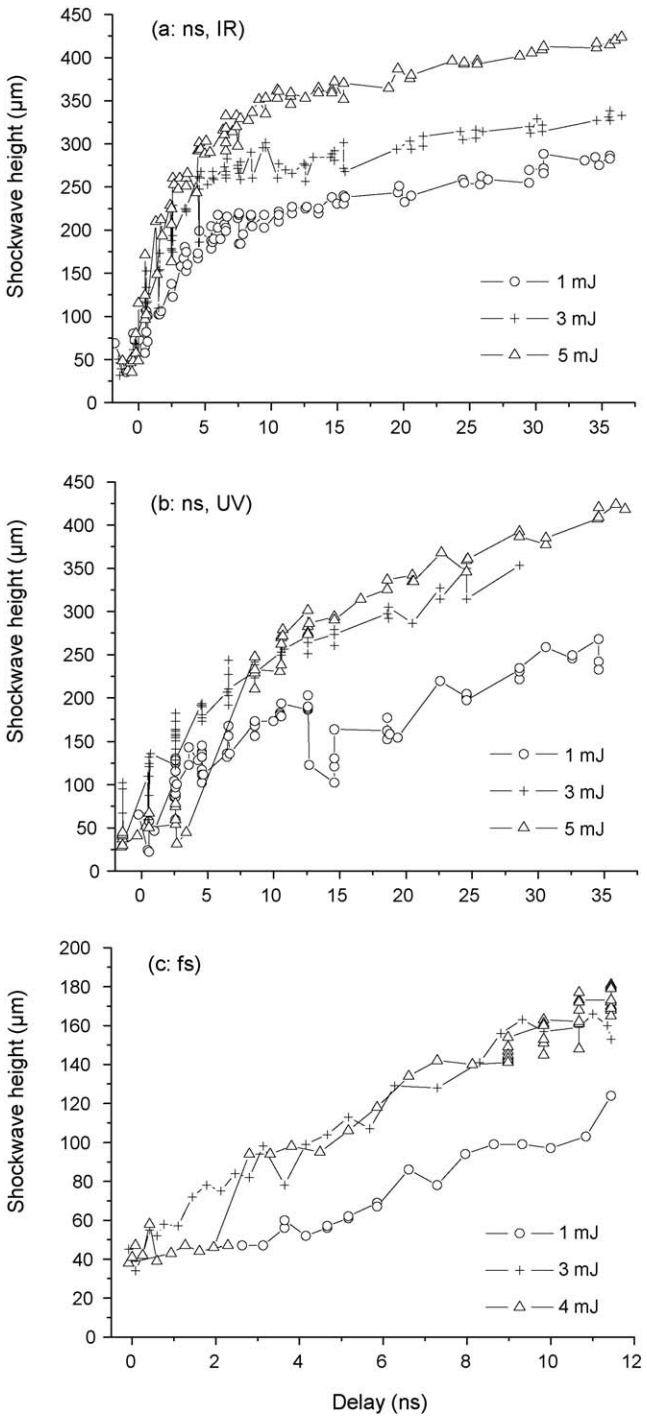

Fig. 4. Heights of shockwaves associated to the plasmas induced on the surface of a nylon sample by nanosecond IR (1064 nm, a), UV (266 nm, b), and femtosecond IR (800 nm, c) laser pulses, with pulse energies of 1, 3 and 5 mJ for the case of nanosecond pulses, and 1, 3 and 4 mJ for the case of femtosecond pulses.

molecules indicates the contribution from the recombination between atomic or molecular carbon in the plasma and nitrogen molecules in air. Such recombination has been observed in different circumstances [11,15–19]. Recombination time constant of several hundreds of nanoseconds can be well fitted by considering involved chemical reactions $C_2 + N_2 \rightarrow 2CN$ and $2C + N_2 \rightarrow 2CN$ [15,16,20].

In Fig. 5a we can see that for the nanosecond IR ablation, signal from CN molecules is rather weak for low laser energies. Efficient production of CN molecules is due to the recombination with ambient air. Such recombination becomes more important for high

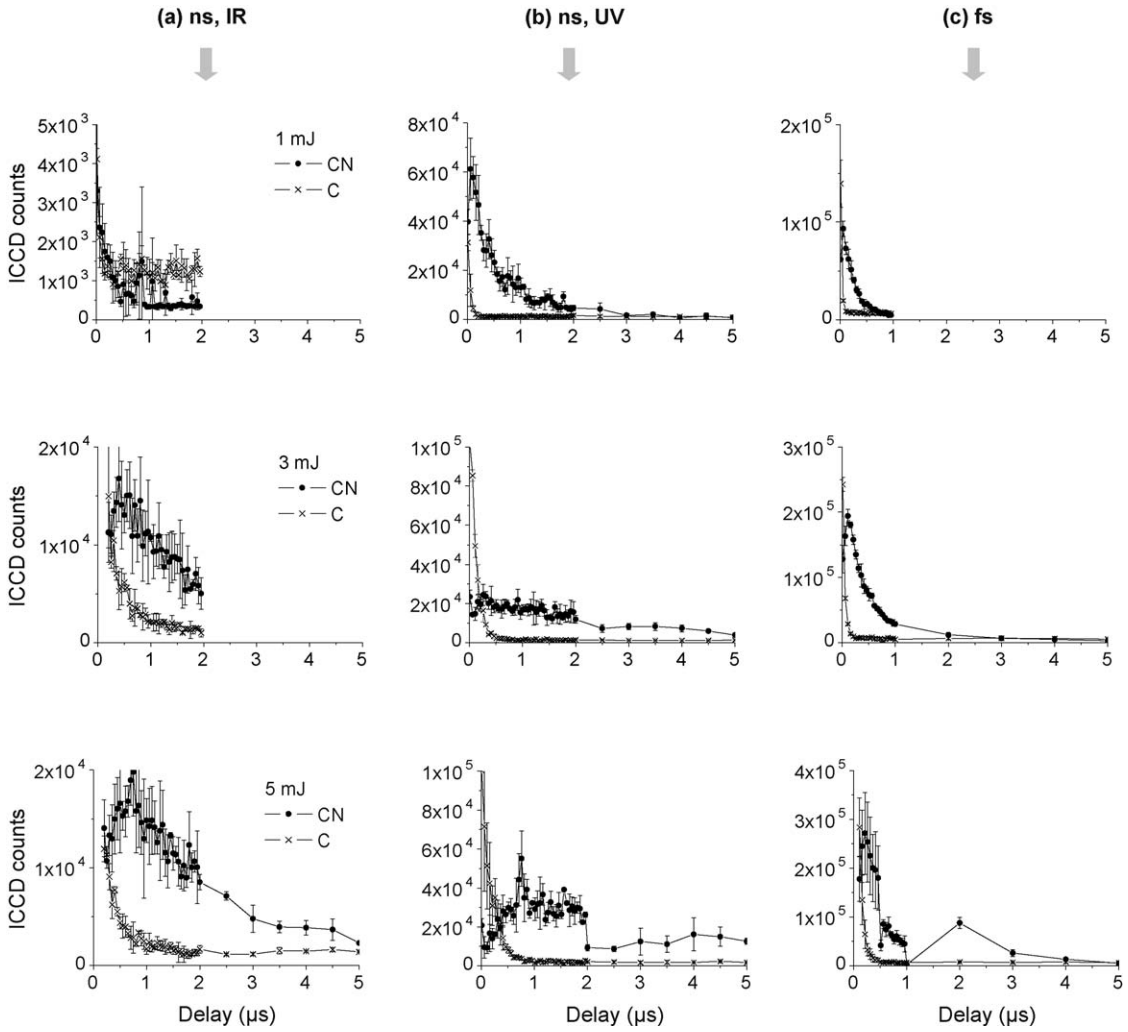

Fig. 5. Time evolutions of emissions of atomic carbon C and molecular radicals CN from plasmas induced by nanosecond IR (a), nanosecond UV (b), and femtosecond (c) laser pulses on the surface of a nylon sample with pulse energy of 1, 3 and 5 mJ.

pulse energies. As we already see in the Section 3.1 with shadowgraphs, for these energies, tailing part of laser pulse is strongly absorbed by the plasma. Absorption of laser energy by the plasma increases the temperature of the plasma, and in turn, its reaction rate with the ambient air due to an increased collision energy [21]. This observation leads to the conclusion that the nanosecond IR ablation regime is not suitable for analysis of organic materials using LIBS with molecular emission, because of its low efficiency to produce native molecular fragments and high rate of recombination with ambient air.

For the nanosecond UV ablation (Fig. 5b), we can see an efficient production of native CN molecules with weak laser energies. This production decreases when energy increases. The recombination with ambient air is observed for high laser energies. For low energy nanosecond UV ablations, the dominant process is photochemical ablation [22]. High energy of UV photon (4.66 eV) allows efficient photoionization of material and direct bond breaking leading to non-thermal ablation and efficient generation of molecular fragments [23–25]. When laser pulse energy is increased and as there is not shielding of laser pulse by plasma, energy coupled to the sample increases, leading to higher plasma temperature and higher atomization degree in the plasma due to photothermal process. Recombination with ambient air becomes important with respect to the production of native molecules. From these observations, we can conclude that low fluence nanosecond UV ablation is quite suitable for an efficient analysis of organic or biological materials with LIBS under atmospheric pressure by providing efficient molecular ablation and allowing low interference due to the recombination with ambient air.

For the femtosecond ablation, Fig. 5c shows efficient molecular ablation for all the three used energies with increasing initial molecular emission intensity for increasing pulse energy. For low pulse energies (1 and 3 mJ), the contribution from recombination is negligible. For 5 mJ, signal due to recombination can be observed for long delays. This is quite similar to the results obtained in the nanosecond UV ablation regime with however, a significantly higher production rate of native CN molecules. In fact, as already shown by the shadowgraphs, in femtosecond ablation, there is no post-ablation interaction between plasma and laser pulse. And due to its high intensity, photochemical ablation is a dominant process through multiphoton ionization and direct bond breaking [26]. As for the nanosecond UV ablation, the femtosecond ablation also allows efficient LIBS analysis of organic and biological samples using molecular emission without interference due the recombination with atmospheric air.

4. Conclusion

We have studied the early stage expansion and the subsequent spectral emission of the plasma induced on the surface of a nylon sample in different laser ablation regimes in terms of pulse duration, wavelength and fluence, in order to identify optimized ablation

regimes for LIBS analysis of organic and biological materials under the atmospheric pressure. Our results demonstrate that an optimized ablation regime can be found with an efficient production of native molecular fragments and a minimized recombination with ambient air. This regime can be provided by either nanosecond UV pulses with low fluence or femtosecond pulses. Nanosecond IR laser is not suitable for organic material analysis using molecular emission, because there is a low molecule production rate at low fluence; and at high fluence the absorption of laser energy by the plasma lead to shielding of the pulse and heating of the plasma. We have observed the correlation between the LSD and the high rate of recombination with ambient air for this regime. For nanosecond UV laser pulses at high fluence, energy deposited on the sample increases because the absence of pulse shielding by the plasma. The important energy deposited on the sample increases the initial energy of the plasma which leads to a higher atomization degree and a reduced molecule production. The recombination rate with ambient air is also increased due to higher collision energies. For the femtosecond ablation, the recombination is observed at high laser energy, while the initial native molecular fragment production remains always high for increasing laser energy in this regime. Compared to the nanosecond ablations, the femtosecond regime offers the highest production rate of molecular fragments. However for application purposes, the use of a nanosecond UV laser with a much more compact and reliable system is obviously advantaged compared to a femtosecond laser who remains actually still more complicate to operate.

Acknowledgement

The authors thank the France Berkeley Funding for the supports.

References

[1] A.W. Mizioley, V. Palleschi, I. Schchter (Eds.), Laser-Induced Breakdown Spectroscopy (LIBS): Fundamentals and Applications, Cambridge University Press, New York, 2006, , ISBN-13 978-0-521-85274-6.
[2] David A. Cremers, Leon J. Radziemski, Handbook of Laser-Induced Breakdown Spectroscopy, Wiley, 2006.
[3] F.C. De Lucia Jr., R.S. Harmon, K.L. McNesby, R.J. Wonkel Jr., A.W. Miziolek, Appl. Opt. 42 (2003) 6148.
[4] C. Lopez-Moreno, S. Palanco, J.J. Laserna, F. DeLucia Jr., A. Miziolek, J. Rose, R.A. Walter, A.I. Whitehouse, J. Anal. Atom. Spectrom. 21 (2006) 55.
[5] J.D. Hybl, G.A. Lithgow, S.G. Buckley, Appl. Spectrosc. 57 (2003) 1207.
[6] A.C. Samuels, F.C. De Lucia Jr., K.L. McNesby, A.W. Miziolek, Appl. Opt. 42 (2003) 6205.
[7] S. Morel, N. Leon, P. Adam, J. Amouroux, Appl. Opt. 42 (2003) 6184.
[8] M. Baudelet, J. Yu, M. Bossu, J. Jovelet, J.-P. Wolf, T. Amodeo, E. Fréjafon, P. Laloi, Appl. Phys. Lett. 89 (2006) 163903.
[9] M. Baudelet, L. Guyon, J. Yu, J.-P. Wolf, T. Amodeo, E. Fréjafon, P. Laloi, Appl. Phys. Lett. 88 (2006) 063901.
[10] M. Baudelet, M. Boueri, J. Yu, S.S. Mao, V. Piscitelli, X. Mao, R.E. Russo, Spectrochim. Acta B 62 (2007) 1329.
[11] M. Baudelet, L. Guyon, J. Yu, J.-P. Wolf, T. Amodeo, E. Fréjafon, P. Laloi, J. Appl. Phys. 99 (2006) 084701.
[12] Y.B. Zel'dovich, Y.P. Raizer, Physics of Shock Waves and High-Temperature Hydrodynamic Phenomena, Dover Publications, Mineola, New York, 2002 .
[13] M. Capitelli, C.M. Ferreira, B.F. Gordiets, A.I. Osipov, Plasma Kinetics in Atmospheric Gases, Springer-Verlag, Berlin, Heidelberg, New York, 2000.
[14] S. De Falco, Interaction laser femtoseconde-métal: Etude expérimentale des mécanismes d'ablation et de formation des nanoparticules, Ph.D. Thesis, Université d'Aix-Marseille II, 2008.
[15] C. Vivien, J. Hermann, A. Perrone, C. Boulmer-Leborgne, A. Luches, J. Phys. D 31 (1998) 1263.
[16] L. St-Onge, R. Sing, S. Béchard, M. Sabsabi, Appl. Phys. A: Mater. Sci. Process 69 (1999) S913.
[17] S. Abdelli-Messaci, T. Kerja, A. Bendib, S. Malek, J. Phys. D 35 (2002) 2772.
[18] R.K. Thareja, R.K. Dwivedi, K. Ebihara, Nucl. Instrm. Meth. Phys. Res. B 192 (2002) 301.
[19] S. Trusso, E. Barletta, F. Barreca, F. Neri, Appl. Phys. A 79 (2004) 1997.
[20] M. Baudelet, Propriétés physico-chimiques du plasma induit par laser en régimes nanoseconde et femtoseconde: Applications analytiques aux bactéries et aux produits agro-alimentaires, Ph.D. Thesis, Université Lyon 1, 2008.
[21] A.R. Hochstim, Kinetic Processes in Gases and Plasmas, Academic Press, 1969.
[22] D. Bäuerle, Laser Processing and Chemistry, 3rd edition, Springer, 2000.
[23] N. Bityurin, B.S. Luk'yanchuk, M.H. Hong, T.C. Chong, Chem. Rev. 103 (2003) 519.
[24] T. Lippert, J.T. Dickinson, Chem. Rev. 103 (2003) 453.
[25] M. Kuhnke, L. Cramer, P.E. Dyer, J.T. Dickinson, T. Lippert, H. Niino, M. Pervolaraki, C.D. Walton, A. Wokaun, J. Phys. 59 (2007) 625.
[26] J. Bonse, S. Baudach, J. Krüger, W. Kautek, M. Lenzner, Appl. Phys. A 74 (2002) 19.